Nonadiabatic Proton-Coupled Electron Transfer Reactions: Impact of Donor−Acceptor Vibrations, Reorganization Energies, and Couplings on Dynamics and Rates

Elizabeth Hatcher, Alexander Soudackov, and Sharon Hammes-Schiffer*

Department of Chemistry, The Pennsylvania State University, 104 Chemistry Building, University Park, Pennsylvania 16802

Received: June 1, 2005; In Final Form: July 29, 2005

Fundamental aspects of proton-coupled electron transfer (PCET) reactions in solution are analyzed with molecular dynamics simulations for a series of model systems. The analysis addresses the impact of the solvent reorganization energy, the proton donor−acceptor mode vibrational frequency, and the distance dependence of the nonadiabatic coupling on the dynamics of the reaction and the magnitude of the rate. The rate for nonadiabatic PCET is expressed in terms of a time-dependent probability flux correlation function. The time dependence of the probability flux correlation function is determined mainly by the solvent reorganization energy and is not significantly influenced by the proton donor−acceptor frequency or the distance dependence of the nonadiabatic coupling. The magnitude of the PCET rate becomes greater as the solvent reorganization energy decreases, the proton donor−acceptor frequency decreases, and the distance dependence of the nonadiabatic coupling increases. The approximations underlying a previously derived analytical PCET rate expression are also investigated. The short-time approximation for the solvent is valid for these types of systems. In addition, solvent damping effects on the proton donor−acceptor motion are not significant on the time scale of the probability flux. The rates calculated from the molecular dynamics simulations agree well with those calculated from the analytical rate expression.

I. Introduction

Proton-coupled electron transfer (PCET) reactions, which involve the simultaneous transfer of an electron and a proton, play a significant role in many chemical and biological processes.[1−18] A variety of theoretical formulations have been applied to PCET reactions.[19−36] Typically PCET reactions are nonadiabatic because of the large distance between the electron donor and acceptor and the small overlap between the localized proton vibrational wave functions for the reactant and product vibronic states. In this regime, the reaction rate is determined by solvent fluctuations, which lead to degeneracy of the reactant and product vibronic states, and by the nonadiabatic coupling, which depends strongly on the proton donor−acceptor separation. Most of the previous studies of PCET reactions neglected the dynamical aspects of the proton donor−acceptor mode and the solvent or protein.

Recently, we derived a dynamical nonadiabatic rate expression for PCET reactions in condensed phases.[29,37] The nonadiabatic rate constant is expressed in terms of the time integral of a time-dependent probability flux correlation function. This rate constant expression includes the dynamical fluctuations of the nonadiabatic coupling and the energy gap between the reactant and product states. The donor−acceptor mode can be treated classically or quantum mechanically. This approach accounts for dynamical correlations between the fluctuations of the proton donor−acceptor distance and the nonadiabatic PCET coupling. Rate expressions were derived for PCET reactions in a number of well-defined limits for both dielectric continuum and molecular representations of the environment. The effects of the proton donor−acceptor and solvent dynamics on this probability flux correlation function were analyzed with classical molecular dynamics simulations.[37]

In this paper, we perform molecular dynamics simulations on model PCET systems to analyze the dependence of the PCET rate on key physical properties of the system and to test the validity of the approximations underlying previously derived rate expressions. The effects of the solvent reorganization energy, the proton donor−acceptor frequency, and the distance dependence of the nonadiabatic coupling on the probability flux correlation function are analyzed by varying the parameters in the model systems. The impact of these properties on the magnitude of the PCET rate constant is also examined. The linear response approximation and the other main approximations underlying previously derived analytical rate expressions are tested for these model systems. The rates calculated from the molecular dynamics simulations are compared to those calculated with an analytical rate expression.

An outline of the paper is as follows. Section II summarizes the theoretical formulation for PCET reactions and describes the model systems. Section III presents the analyses of the dependence of the probability flux correlation function on key physical properties of the system and the main approximations underlying previously derived rate expressions. The conclusions and future directions are given in section IV.

II. Methods

A. Theoretical Formulation. PCET systems may be described in terms of the proton coordinate r_p, the proton donor−acceptor coordinate R, and the solvent coordinates ξ. In our theoretical formulation for nonadiabatic PCET reactions,[26,27] the active electrons and transferring proton are treated quantum mechanically. The PCET reaction is described in terms of

* Corresponding author. E-mail: shs@chem.psu.edu.

10.1021/jp052909f CCC: $30.25
Published on Web 09/08/2005

nonadiabatic transitions between pairs of reactant (Iμ) and product (IIν) electron−proton vibronic states. Here I and II, respectively, denote the sets of reactant and product diabatic states, and μ and ν denote vibronic states within each set. The reactant vibronic surfaces $\epsilon_\mu^{\mathrm{I}}(R,\xi)$ and product vibronic surfaces $\epsilon_\nu^{\mathrm{II}}(R,\xi)$ are obtained by calculating the proton vibrational states for the reactant and product ET electronic states.

In our previous work,[26,27] the solute is represented by a four-state valence bond (VB) model.[38] For PCET reactions involving the transfer of one electron and one proton, the four diabatic electronic basis states are

$$\begin{aligned}
&(1a)\quad \mathrm{D_e}^-\cdots\cdots\mathrm{D_pH}^+\cdots\cdots\mathrm{A_p}\cdots\cdots\mathrm{A_e}\\
&(1b)\quad \mathrm{D_e}^-\cdots\cdots\mathrm{D_p}\cdots\cdots{}^+\mathrm{HA_p}\cdots\cdots\mathrm{A_e}\\
&(2a)\quad \mathrm{D_e}\cdots\cdots\mathrm{D_pH}^+\cdots\cdots\mathrm{A_p}\cdots\cdots\mathrm{A_e}^-\\
&(2b)\quad \mathrm{D_e}\cdots\cdots\mathrm{D_p}\cdots\cdots{}^+\mathrm{HA_p}\cdots\cdots\mathrm{A_e}^-
\end{aligned} \tag{1}$$

where 1 and 2 denote the ET state and *a* and *b* denote the PT state. Typically the solvated 1*a* and 2*b* states are lower in energy than the intermediate states 1*b* and 2*a* because the electrostatic interactions within the complex dominate over the solvation energies for bulky complexes.[39] Therefore, the reactant ET state is predominantly 1*a*, and the product ET state is predominantly 2*b*.

The coupling $V_{\mu\nu}$ between two vibronic states Iμ and IIν is defined as

$$V_{\mu\nu} = \langle\phi_\mu^{\mathrm{I}}|V(r_{\mathrm{p}},\xi^\dagger)|\phi_\nu^{\mathrm{II}}\rangle_{\mathrm{p}} \tag{2}$$

In eq 2, the subscript of the angular brackets indicates integration over r_{p}, $\xi^\dagger$ represents the solvent coordinates at the intersection point of the reactant and product surfaces along the line connecting the minima of the surfaces, $V(r_{\mathrm{p}},\xi)$ is the electronic coupling between reactant and product states, and ϕ_μ^{I} and ϕ_ν^{II} are the proton vibrational wave functions for the reactant and product vibronic states, respectively. For many PCET systems,[40,41] the coupling is approximately of the form

$$V_{\mu\nu} \approx V^{\mathrm{el}}\langle\phi_\mu^{\mathrm{I}}|\phi_\nu^{\mathrm{II}}\rangle_{\mathrm{p}} \tag{3}$$

where V^{el} is a constant effective electronic coupling and $\langle\phi_\mu^{\mathrm{I}}|\phi_\nu^{\mathrm{II}}\rangle_{\mathrm{p}}$ is the overlap between the reactant and product vibrational wave functions. The nonadiabatic coupling depends strongly on the proton donor−acceptor coordinate *R* because this coordinate modulates the proton tunneling distance and therefore the overlap $\langle\phi_\mu^{\mathrm{I}}|\phi_\nu^{\mathrm{II}}\rangle_{\mathrm{p}}$. Although the coupling does not depend explicitly on the solvent coordinates in the relevant regime, the fluctuations of the solvent degrees of freedom can be dynamically coupled to the *R* motion, which in turn impacts the fluctuations of the nonadiabatic coupling.

Recently we developed nonadiabatic PCET rate expressions that include the dynamical effects of both the proton donor−acceptor motion and the solvent.[29] In this formulation, the electrons and transferring proton are adiabatic with respect to the *R* coordinate and the solvent within the reactant and product states, and the *R* mode is treated dynamically on the same level as the solvent modes. The nonadiabatic dynamical rate constant can be expressed as

$$k^{\mathrm{dyn}} = \sum_\mu^{\{\mathrm{I}\}} P_\mu^{\mathrm{I}} \sum_\nu^{\{\mathrm{II}\}} k_{\mu\nu}^{\mathrm{dyn}} \tag{4}$$

where P_μ^{I} is the Boltzmann weighting for the reactant state Iμ and $k_{\mu\nu}^{\mathrm{dyn}}$ is the partial rate constant describing nonadiabatic transitions between the reactant (Iμ) and product (IIν) vibronic states. The partial rate constant $k_{\mu\nu}^{\mathrm{dyn}}$ is the integral of the time-dependent probability flux correlation function $j_{\mu\nu}(t)$:

$$k_{\mu\nu}^{\mathrm{dyn}} = \frac{1}{\hbar^2}\int_{-\infty}^{\infty} j_{\mu\nu}(t)\,\mathrm{d}t \tag{5}$$

The probability flux correlation function $j_{\mu\nu}(t)$ can be represented in terms of the Heisenberg operators describing the time evolution of the energy gap and the coupling.[29] To facilitate the derivation of an analytical expression for the probability flux correlation function, the *R* dependence of the overall coupling $V_{\mu\nu}$ is approximated by a single exponential:

$$V_{\mu\nu} \approx V_{\mu\nu}^{(0)} \exp[-\alpha_{\mu\nu}(R - \bar{R}^{\mathrm{I}\mu})] \tag{6}$$

where $\bar{R}^{\mathrm{I}\mu}$ is the equilibrium value of the *R* coordinate on the reactant surface Iμ, $V_{\mu\nu}^{(0)}$ is the value of the coupling at $R = \bar{R}^{\mathrm{I}\mu}$, and $\alpha_{\mu\nu}$ can be estimated from the *R* dependence of the coupling. The justification for eq 6 is that the nonadiabatic coupling can be approximated as the product of a constant electronic coupling and the overlap of the reactant and product proton vibrational wave functions, as given in eq 3. For a simple model based on two ground-state harmonic oscillator wave functions with centers separated by *R*, the overlap increases exponentially with decreasing *R*. A more detailed justification for eq 6 is provided in ref 37. The approximation in eq 6 has been shown to be reasonable for model PCET systems and was also used previously for nonadiabatic proton transfer systems.[42−44]

Performing a second-order cumulant expansion, the probability flux correlation function is expressed as

$$\begin{aligned}
j_{\mu\nu}(t) = |V_{\mu\nu}^{(0)}|^2 \exp\left[\frac{i}{\hbar}\langle\epsilon_{\mu\nu}\rangle t\right] \times \exp\Bigg\{&\alpha_{\mu\nu}^2[C_R(0) + C_R(t)] - \\
&\frac{2i\alpha_{\mu\nu}}{\hbar}\langle\tilde{D}_{\mu\nu}\rangle\int_0^t C_R(\tau)\mathrm{d}\tau - \frac{1}{\hbar^2}\int_0^t \mathrm{d}\tau_1\int_0^{\tau_1}\mathrm{d}\tau_2 C_\epsilon(\tau_1-\tau_2) - \\
&\frac{1}{\hbar^2}\int_0^t \mathrm{d}\tau_1\int_0^{\tau_1}\mathrm{d}\tau_2 C_D(\tau_1-\tau_2)C_R(\tau_1-\tau_2)\Bigg\}
\end{aligned} \tag{7}$$

where the time evolution on the reactant vibronic surface is described in terms of the energy gap coordinate

$$\epsilon_{\mu\nu}(t) = \epsilon_\nu^{\mathrm{II}}(\bar{\mathrm{R}}^{\mathrm{I}\mu},\xi) - \epsilon_\mu^{\mathrm{I}}(\bar{\mathrm{R}}^{\mathrm{I}\mu},\xi) \tag{8}$$

the derivative of the energy gap

$$\tilde{D}_{\mu\nu}(t) = \left.\frac{\partial\epsilon_{\mu\nu}}{\partial R}\right|_{R=\bar{R}^{\mathrm{I}\mu}} \tag{9}$$

and the *R* mode. Note that these quantities are evaluated at $R = \bar{R}^{\mathrm{I}\mu}$ because the energy gap is expanded about $R = \bar{R}^{\mathrm{I}\mu}$ in the derivation of the rate expression.[29] The time correlation functions $C_\epsilon(t)$, $C_R(t)$, and $C_D(t)$ are defined as

$$\begin{aligned}
C_\epsilon(t) &= \langle\delta\epsilon_{\mu\nu}(0)\delta\epsilon_{\mu\nu}(t)\rangle\\
C_R(t) &= \langle\delta R(0)\delta R(t)\rangle\\
C_D(t) &= \langle\tilde{D}_{\mu\nu}(0)\tilde{D}_{\mu\nu}(t)\rangle
\end{aligned} \tag{10}$$

where $\delta\epsilon_{\mu\nu}(t) = \epsilon_{\mu\nu}(t) - \langle\epsilon_{\mu\nu}\rangle$ and $\delta R(t) = R(t) - \langle R\rangle$. This

formulation of the rate expression is similar to that previously derived for vibrationally nonadiabatic PT reactions occurring on a single adiabatic electronic surface.[42−45]

If the potential energy of the system is assumed to be harmonic along the R coordinate, the energy gap derivative defined in eq 9 becomes the constant

$$\tilde{D}_{\mu\nu} = \tilde{\Lambda}_{\mu\nu} \equiv -M\Omega^2\Delta R_{\mu\nu} \tag{11}$$

where $\Delta R = \bar{R}^{\mathrm{II}\nu} - \bar{R}^{\mathrm{I}\mu}$ is the difference between the equilibrium R coordinates on the product and reactant surfaces, and the R mode frequency Ω is given by

$$M\Omega^2 = \left.\frac{\partial^2 \epsilon_\mu^{\mathrm{I}}(R,\xi)}{\partial R^2}\right|_{R=\bar{R}^{\mathrm{I}\mu}} \tag{12}$$

In this limit, the energy gap derivative is independent of time, so $\langle\tilde{D}_{\mu\nu}\rangle = \tilde{\Lambda}_{\mu\nu}$ and $C_D(t) = \tilde{\Lambda}_{\mu\nu}^2$. For a symmetric system, $\tilde{\Lambda}_{\mu\nu} = 0$. As shown in ref 37, often the two terms in eq 7 that include this factor are negligible relative to the other terms due to the relatively small magnitude of $\langle\tilde{D}_{\mu\nu}\rangle$. In this paper, however, we do not assume harmonicity of the potential energy along the R coordinate, and we include all terms in our calculations of the nonadiabatic rates.

Classical molecular dynamics simulations of the full solute−solvent system on the reactant vibronic surface $\epsilon_\mu^{\mathrm{I}}(R,\xi)$ can be used to calculate the input quantities for eq 7. The $C_R(t)$ term is calculated from molecular dynamics simulations with an unconstrained R, and the $\langle\epsilon_{\mu\nu}\rangle$, $\langle\tilde{D}_{\mu\nu}\rangle$, $C_\epsilon(t)$, and $C_D(t)$ terms are calculated from molecular dynamics simulations with the R coordinate constrained to $R = \langle R\rangle$, where $\langle R\rangle$ is obtained from the unconstrained simulation. (Note that we assumed $\bar{R}^{\mathrm{I}\mu} = \langle R\rangle$ in the derivation of the rate expression.) In the molecular dynamics simulations, the transferring proton is bound to the proton donor at a fixed distance corresponding to the reactant. For the calculation of the energy gap, the product state energy is obtained by moving the proton so that it is bound to the proton acceptor at the same fixed distance. This approximation neglects the effects of delocalization of the hydrogen nuclear wave function on the motion of the other nuclei.

Although the proton nucleus is described classically in the molecular dynamics simulations, the quantum mechanical nature of the proton is implicitly included in the nonadiabatic rate expression through the nonadiabatic couplings between the reactant and product vibronic states. As shown in eq 3, these couplings depend on the overlap between the reactant and product proton vibrational wave functions and thus are inherently quantum mechanical. The magnitude and distance dependence of the couplings in eq 6 could be fit to couplings obtained from purely quantum mechanical calculations using the nuclear-electronic orbital approach.[46,47]

The quantum mechanical behavior of the R motion can also be included in the nonadiabatic rate expression using the standard analytical expression for the time correlation function of an undamped quantum mechanical harmonic oscillator for $C_R(t)$:[48]

$$C_R(t) = \frac{\hbar}{2M\Omega}\left[\coth\left(\left(\frac{1}{2}\right)\beta\hbar\Omega\right)\cos\Omega t + i\sin\Omega t\right] \tag{13}$$

In eq 13, the R coordinate motion is assumed to be harmonic, and the solvent damping effects on this harmonic motion are neglected. The classical (high temperature) analogue of this expression is

$$C_R(t) = \frac{1}{\beta M\Omega^2}\cos\Omega t \tag{14}$$

TABLE 1: Calculated Quantities from the Molecular Dynamics Simulations for the Three Models

	model 1	model 2	model 3
$\langle R\rangle$, Å	2.83	2.92	2.85
Ω, cm^{-1}	387	198	388
$\langle\epsilon\rangle$, kcal/mol	53.1	56.1	29.9
$\langle\delta\epsilon^2\rangle/2k_BT$, kcal/mol	65.3	66.7	35.0
$\tilde{D}$, kcal/(mol·Å)	3.9	3.8	2.4

B. Model System. The probability flux correlation function is affected by changes in the proton donor−acceptor vibrational frequency (Ω), the solvent reorganization energy ($\lambda = \langle\epsilon_{\mu\nu}\rangle$ for a symmetric system), and the distance dependence of the coupling ($\alpha_{\mu\nu}$). In this paper, we focus on nonadiabatic transitions between the lowest energy reactant and product states (i.e., include only $\mu = \nu = 0$ in the rate expression given in eq 4). For notational simplicity, we drop the μ and ν subscripts for the remainder of the paper. We studied three symmetric model systems with different values of Ω and λ to examine the impact of these properties on the probability flux correlation function. The parameters of the three model systems are given in Table 1. For each of these model systems we calculated the rate with α = 5, 10, 15, 20, 25, and 30 Å^{-1}.

The basic PCET model system consists of an electron donor and acceptor, a proton donor and acceptor, and a transferring proton. This model system is depicted in Figure 1. The masses of the electron donor and acceptor are 100.0 g/mol, and the masses of the proton donor and acceptor are 14.0 g/mol. To maintain approximate linearity, harmonic restraints with force constants of 100.0 kcal/(mol·deg^2) and equilibrium values of 180° are applied to the $D_eD_pA_e$ angle, the $D_eA_pA_e$ angle, and the D_pHA_p angle. The D_e-A_e distance is constrained to 8 Å, and the D_p-H distance is constrained to 1.1 Å. The potentials between the D_e-D_p, A_e-A_p, and D_p-A_p coordinates are represented as three coupled harmonic oscillators with identical force constants. The equilibrium distances for these harmonic potentials are 2.6 Å for D_e-D_p and A_e-A_p and 2.8 Å for D_p-A_p. The proton donor−acceptor vibrational frequency Ω is varied by changing the force constants for these harmonic potentials. The force constants for the harmonic potentials are 63.3 kcal/(mol·Å^2) for models 1 and 3 and 15.8 kcal/(mol·Å^2) for model 2. For the simulations with a constrained R distance, the D_p-A_p distance is constrained to $\langle R\rangle$, the average R distance obtained from the unconstrained simulations. The values of $\langle R\rangle$ are given in Table 1.

The solute is solvated with 253 flexible TIP3P[49−51] water molecules in a cubic box with sides of 19.34 Å^3. The solvent−solute interactions include both electrostatic and van der Waals interactions. For the reactant state, the electron donor and acceptor have charges of −0.5 and +0.5 e, respectively, and the proton donor and acceptor have charges of 0.0 and −0.5 e, respectively. For the product state, the charges on the donors and acceptors are reversed. The proton always has a charge of +0.5 e. These charges were chosen to ensure an overall neutral charge for the solute. The long-range electrostatic interactions in the periodic system are treated with the Ewald method.[52] The van der Waals pair parameters for the interactions of the proton donor and acceptor with the oxygen atoms of the water molecules are ϵ = 0.15595 kcal/mol and σ = 4.1416 Å. The reorganization energy λ is varied by changing the van der Waals

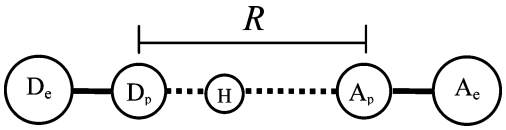

Figure 1. Schematic picture of the solute for the model PCET system.

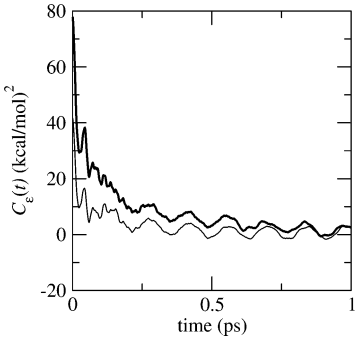

Figure 2. Energy gap correlation function $C_\epsilon(t)$ for model 1 (thick line) and model 3 (thin line). $C_\epsilon(0)$ is larger for model 1 because model 1 has a larger solvent reorganization energy.

parameter σ of the electron donor and acceptor, where increasing the radii of the electron donor and acceptor decreases the solvent−solute electrostatic interactions and thereby decreases the solvent reorganization energy. The van der Waals pair parameters for the interactions of the electron donor and acceptor with the oxygen atoms of the water molecules are $\epsilon = 0.055$ kcal/mol for all three models and $\sigma = 4.075$ Å for models 1 and 2 and $\sigma = 5.075$ Å for model 3.

All of the molecular dynamics simulations were performed with a modified version of DL_POLY 2.14.[53] The classical equations of motion were integrated with the Verlet leapfrog algorithm[54] with a time step of 0.5 fs. The solute constraints were applied with the SHAKE algorithm.[55] A canonical ensemble with a temperature of 300 K was maintained with a Nose-Hoover thermostat with a relaxation time of 0.4 ps.[56] The system was equilibrated for 100 ps, and the data was collected for 200 ps. We verified that the results were converged by extending the simulation for model 1 to 1 ns.

III. Results and Discussion

A. Impact of Physical Properties on Dynamics and Rates. In this subsection, we analyze the contributions to the probability flux correlation function given in eq 7. For this purpose, we performed molecular dynamics simulations for the three different model systems described above. These model systems enable us to examine the impact of the solvent reorganization energy, proton donor−acceptor frequency, and distance dependence of the coupling on the probability flux correlation function and the magnitude of the rate.

The energy gap and R coordinate correlation functions provide insight into the relative time scales of the solvent and proton donor−acceptor motions. The energy gap correlation functions $C_\epsilon(t)$ for models 1 and 3 are depicted in Figure 2. $C_\epsilon(t)$ exhibits two different relaxation times: an initial fast decay on the time scale of ∼50 fs and a slower exponential decay on a time scale of ∼0.5 ps. The fast and slow components of the decay of the energy gap correlation function correspond to the relatively high-frequency librational modes of water and the lower frequency rotational and translational modes of water, respectively. Since model 1 has a larger solvent reorganization energy than model 3, $C_\epsilon(0) = \langle \delta\epsilon^2 \rangle$ is larger for model 1. The R coordinate correlation functions $C_R(t)$ for models 1 and 2 are depicted in Figure 3. The R coordinate correlation function is highly

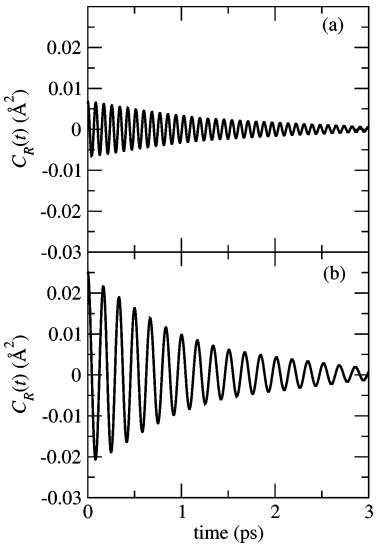

Figure 3. Proton donor−acceptor distance correlation function $C_R(t)$ for (a) model 1 and (b) model 2. The amplitude and period of the oscillations of $C_R(t)$ are smaller for model 1 because model 1 has a larger proton donor−acceptor vibrational frequency.

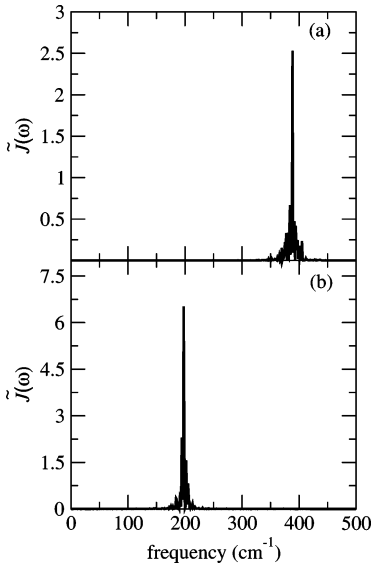

Figure 4. Normalized spectral density $\tilde{J}(\omega)$ of the R-coordinate time correlation function $C_R(t)$ defined in eq 16 for (a) model 1 and (b) model 2. The peak in the spectral density corresponds to the average frequency of the proton donor−acceptor vibrational mode.

oscillatory and decays on a slower time scale of ∼3 ps due to the weak coupling of the R motion to the solvent degrees of freedom. The amplitude and the period of the oscillations of the $C_R(t)$ term are larger for model 2 than for model 1 because model 2 has a smaller proton donor−acceptor frequency.

The normalized spectral densities of the R coordinate time correlation functions for models 1 and 2 are depicted in Figure 4. The spectral density $J(\omega)$ is defined in terms of the cosine transform of the time correlation function $C(t)$ as

$$C(t) = \frac{8}{\pi\beta}\int_0^\infty \frac{J(\omega)}{\omega}\cos(\omega t)\,\mathrm{d}\omega \tag{15}$$

and the normalized spectral density is defined as[57]

$$\tilde{J}(\omega) = J(\omega)\Big/\int_0^\infty \frac{J(\omega)}{\omega}\,\mathrm{d}\omega \tag{16}$$

where $\beta = 1/k_B T$. The sharp peaks at ~400 and ~200 cm^{-1} for models 1 and 2, respectively, in the R coordinate spectral density correspond to the proton donor−acceptor vibrational frequency. For an undamped harmonic oscillator, $C_R(t)$ would oscillate indefinitely with fixed amplitude, and the spectral density would be a δ function at the corresponding frequency. The calculated spectral densities of the R coordinate are broadened because the time correlation function $C_R(t)$ is damped due to solute−solvent coupling.

The dominant terms in the probability flux correlation function given in eq 7 are the quantum coherent term

$$F_Q(t) = \exp[(i/\hbar)\langle\epsilon\rangle t]$$

the solvent damping term

$$F_\epsilon(t) = \exp\left[-\frac{1}{\hbar^2}\int_0^t d\tau_1 \int_0^{\tau_1} d\tau_2 C_\epsilon(\tau_1 - \tau_2)\right]$$

and the R coordinate term

$$F_R(t) = \exp\{\alpha^2[C_R(0) + C_R(t)]\}$$

The quantum coherent and solvent damping terms are strongly influenced by changes in the solvent reorganization energy λ. The R-coordinate term is strongly influenced by the proton donor−acceptor vibrational frequency Ω and the parameter α, which describes the distance dependence of the nonadiabatic coupling. The three model systems described in Table 1 will enable us to investigate the impact of solvent reorganization energy, proton donor−acceptor vibrational frequency, and α on the probability flux correlation function. The normalized probability flux correlation functions and the dominant terms for all of the model systems with $\alpha = 10$ Å^{-1} are depicted in Figure 5.

The highly oscillatory function $F_Q(t)$ depicted in Figure 5b is the quantum coherent term, which describes the coherent oscillations of the quantum amplitude between the reactant and product vibronic states. The period of the oscillation for this term is determined by the solvent reorganization energy of the system. The quantum coherent terms for models 1 and 2 have similar periods of ~2 fs because the reorganization energies for these systems are similar. In contrast, the quantum coherent term for model 3 has a larger period of ~3 fs because this system has a smaller solvent reorganization energy. The quantum coherent term is damped by other terms in eq 7, thereby enabling the calculation of a reaction rate.

The solvent damping term $F_\epsilon(t)$ dominates the decay of the probability flux because it decays to zero much faster than any other component in the probability flux. Similar to the coherent term, the solvent damping term depends on the solvent reorganization energy of the system. As illustrated in Figure 5c, the solvent decay terms for models 1 and 2 decay on similar time scales of ~5 fs, whereas the solvent decay term for model 3 decays on a time scale of ~8 fs. The solvent term decays slower for model 3 than for models 1 and 2 because model 3 has a smaller solvent reorganization energy. As a result, the probability flux decays on a slower time scale for model 3 than for model 1 and 2, as depicted in Figure 5a. The magnitude of the rate, which is obtained by time integration of the probability flux correlation function, is smaller for model 1 than for model 3 because model 1 has a larger solvent reorganization energy.

The R coordinate term $F_R(t)$ depicted in Figure 5d depends on the proton donor−acceptor frequency Ω. As shown in Figure 3, the magnitude of $C_R(0) = \langle\delta R^2\rangle$ (i.e., the variance) increases as the proton donor−acceptor frequency decreases. As a result, the magnitude of the R coordinate term increases as the proton donor−acceptor frequency decreases. All of the R coordinate terms have a similar slope on the time scale of the probability flux decay, but the magnitude of the R coordinate term is much larger for model 2 than for models 1 and 3 due to the smaller proton donor−acceptor frequency for model 2. Thus, the magnitudes of the rates calculated for model 2 are larger by 2 orders of magnitude. The normalized probability flux is similar for models 1 and 2, however, indicating that the dynamics of the reaction is not affected by the proton donor−acceptor frequency.

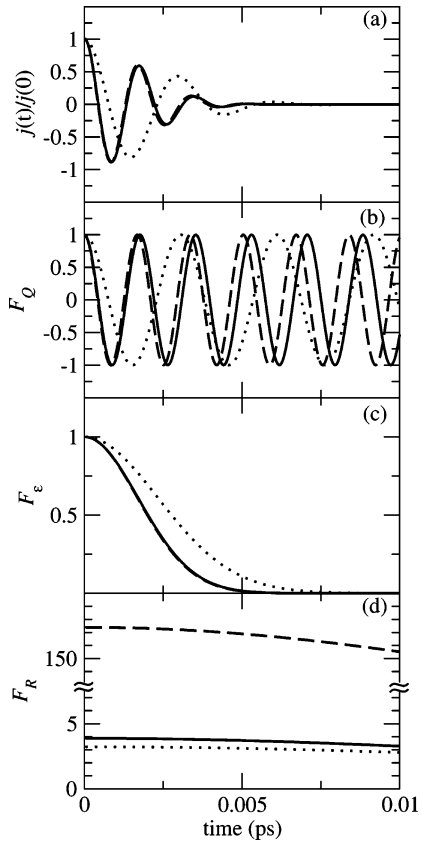

Figure 5. Normalized probability flux correlation function $j(t)/j(0)$ and its dominant components for model 1 (solid), model 2 (dashed) and model 3 (dotted) with $\alpha = 10$ Å^{-1}. (a) normalized probability flux correlation function, (b) quantum coherent term $F_Q(t) = \exp[(i/\hbar)\langle\epsilon\rangle t]$, (c) solvent damping term $F_\epsilon(t) = \exp\{-(1/\hbar^2)\int_0^t d\tau_1 \int_0^{\tau_1} d\tau_2\, C_\epsilon(\tau_1 - \tau_2)\}$, and (d) R-coordinate term $F_R(t) = \exp\{\alpha^2[C_R(0) + C_R(t)]\}$. The normalized probability flux and solvent damping term for models 1 and 2 are nearly indistinguishable because they have similar solvent reorganization energies. Without normalization, the probability flux for models 1 and 2 would not have similar magnitudes due to the different R coordinate terms. The real parts of the complex terms are plotted.

The value of the parameter α also strongly impacts the magnitude of the R coordinate term. Figure 6 depicts the rate as a function of α for all three model systems with $V^{(0)} = 0.1$ kcal/mol. The rate increases with increasing α for all model systems, but the rate increases much faster with α for model 2 because model 2 has a lower proton donor−acceptor frequency. As shown in Figure 3, the smaller R distances are more accessible with a lower proton donor−acceptor frequency. The nonadiabatic coupling increases exponentially as the R distance decreases, thereby dramatically increasing the reaction rate. For small values of α (i.e., $\alpha < 5$), the rate for model 1 is lower than the rate for model 3 because model 1 has a larger solvent

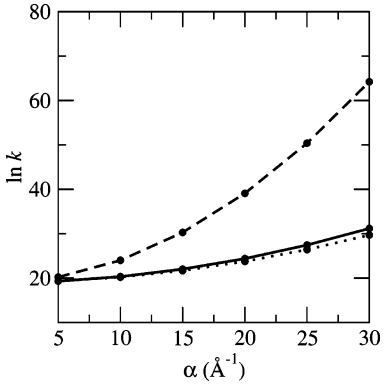

Figure 6. The ln k as a function of α for model 1 (solid), model 2 (dashed), and model 3 (dotted). The rate constant k is given in s^{-1}.

reorganization energy, which influences the solvent damping term as described above. For larger values of α, the rate for model 3 is slightly lower than the rate for model 1 because the F_R term is a little bit lower for model 3, as illustrated in Figure 5d, and this term becomes dominant for large values of α. The physical origin of this phenomenon is that the differences in the van der Waals pair parameters for the solute−solvent interactions in models 1 and 3 slightly impact the R coordinate correlation function as well as the solvent reorganization energy.

B. Analysis of Approximations Underlying Rate Expressions. In the first part of this subsection, we analyze the results of our molecular dynamics simulations to test the validity of the linear response approximation for model PCET systems. In the linear response approximation, the energy gap distribution function $P(\epsilon)$ is a Gaussian characterized by the average $\langle\epsilon\rangle$ and the variance $\langle\delta\epsilon^2\rangle$ of the energy gap reaction coordinate. Here we define the energy gap reaction coordinate as in eq 8, so the average value $\langle\epsilon\rangle$ will be positive for the reactant state and negative for the product state. The free energy is calculated from the distribution function using the standard prescription

$$G(\epsilon) = -k_B T \ln[P(\epsilon)] \tag{17}$$

where k_B is the Boltzmann constant and T is the temperature of the system.[45] In the linear response regime, the free energy curve is a parabola with minimum $\langle\epsilon\rangle$ and force constant

$$f_{harm} = \frac{k_B T}{\langle\delta\epsilon^2\rangle} \tag{18}$$

Marcus theory for electron transfer reactions is based on the linear response approximation.[58] In this theory, the free energy surfaces G_I and G_{II} for the reactant and product states are assumed to be harmonic functions of the energy gap coordinate with identical force constants given in eq 18. The reactant and product free energy surfaces are related to each other as[59,60]

$$G_{II}(\epsilon) = G_I(\epsilon) + \epsilon \tag{19}$$

The corresponding reorganization energy is expressed in terms of the variance as

$$\lambda_{harm} = \frac{\langle\delta\epsilon^2\rangle}{2k_B T} \tag{20}$$

Within the Marcus theory framework, the activation free energy is a simple quadratic function of the reaction free energy $\Delta G°$ (driving force):

$$\Delta G^\dagger = \frac{(\Delta G^0 + \lambda_{harm})^2}{4\lambda_{harm}} \tag{21}$$

and the reaction rate constant is exponentially dependent on the activation free energy:

$$k \propto \exp(-\Delta G^\dagger / k_B T) \tag{22}$$

This expression leads to the Marcus energy gap law, which is manifested by the inverted parabolic dependence of the logarithm of the rate constant on the reaction free energy. An analogous theoretical formulation has been developed for PCET reactions.[26,27]

The energy gap distribution function $P(\epsilon)$ is obtained from our molecular dynamics simulations by binning the energy gap values calculated along the molecular dynamics trajectory over 100 bins spanning the range of energies from 20 to 90 kcal/mol. The calculated distribution for model 1 shown in Figure 7a resembles a Gaussian distribution centered at $\epsilon = \langle\epsilon\rangle$. The reactant free energy curve for model 1, depicted in Figure 7b, is calculated from eq 17. For thermoneutral and symmetrical systems, the product free energy curve $G_{II}(\epsilon)$ can be obtained by reflecting the reactant free energy curve about the y-axis. In this case, the reorganization energy λ is defined as the average value of the energy gap in the reactant state (i.e., $\lambda = \langle\epsilon\rangle$). The calculated values of the reorganization energy for all three model systems are given in Table 1.

These numerical results obtained from molecular dynamics simulations can be compared to results calculated from linear response theory. The harmonic free energy curve obtained from linear response theory (i.e., with the force constant given in eq 18) for model 1 is shown in Figure 7b for comparison to the free energy curve obained from eq 17 with the calculated energy gap distribution function. The nearly harmonic free energy curve, corresponding to a nearly Gaussian form of the energy gap distribution function, indicates that the linear response approximation is reasonable for this system. This observation provides validation for the use of the second-order cumulant expansion in the derivation of the rate expression.

For a quantitative analysis, Table 1 provides a comparison of the reorganization energies calculated from the variance with eq 20 and the reorganization energies calculated from $\lambda = \langle\epsilon\rangle$. The reorganization energies $\lambda = \langle\epsilon\rangle$ are smaller than the corresponding reorganization energies calculated from eq 20 by 23%, 19%, and 17% for models 1, 2, and 3, respectively. These discrepancies arise from slight anharmonicities of the free energy surfaces. We found that these discrepancies decrease as the van der Waals radii of the donors and acceptors are increased. This observation suggests that the deviations from linear response theory arise from short-range solvent−solute interactions that are neglected in the linear response approximation.

We also examine the dependence of the rate constant on the reaction free energy for comparison to the Marcus theory energy gap law. For this purpose, we add the driving force $\Delta G°$ to $\langle\epsilon\rangle$ in the first exponential of the probability flux expression given by eq 7. This process corresponds to shifting the product free energy surface vertically along the free energy axis by $\Delta G°$. The resulting ln k as a function of $\Delta G°$ for model 1 is depicted in Figure 8. This curve is a nearly symmetric inverted parabola with a maximum at $\Delta G° \approx \lambda = \langle\epsilon\rangle = 53.13$ kcal/mol. For comparison, Figure 8 also depicts the symmetric Marcus inverted parabola obtained from the rate constant expression given in eq 22 in conjunction with the activation free energy

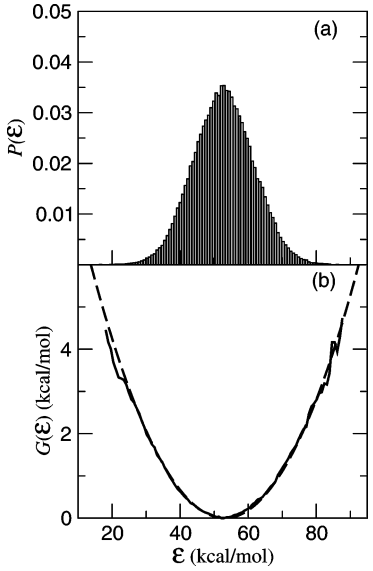

Figure 7. (a) Histogram of the reactant energy gap distribution and (b) the reactant free energy curve calculated from the energy gap distribution with eq 17 (solid) and a parabola calculated from the function $G(\epsilon) = {}^1/_2[(k_BT)/\langle\delta\epsilon^2\rangle](\epsilon - \langle\epsilon\rangle)^2$ (dashed).

given in eq 21 for $\lambda = \langle\epsilon\rangle = 53.13$ kcal/mol. The shape of the Marcus inverted parabola is very similar to the curve obtained by integrating the probability flux correlation function in eq 7. Thus, despite the slight anharmonicity of the free energy surfaces, the calculated energy gap law for this model PCET reaction provides further validation of the linear response approximation for this range of parameters at room temperature.

Deviations of the experimentally measured energy gap laws from the inverted parabolic behavior for electron transfer reactions have been explained by quantum vibronic effects,[61,62] different solute polarizabilities for reactant and product states,[63,64] and solvent nuclear quantum effects.[57,65] The present calculations do not include these additional factors. In particular, we do not account for the quantum effects arising from the excited electron−proton vibronic states, which are included in the general rate expression given in eq 4. These excited states could lead to deviations of the energy gap law from the symmetric inverted parabolic behavior. For typical PCET systems with highly asymmetric proton potentials and relatively large vibronic energy level splittings in the reactant and product electronic states, however, these quantum effects are not expected to be significant.

In the remainder of this subsection, we test the additional approximations underlying the derivation of the following analytical rate expression for nonadiabatic PCET reactions:[29]

$$k^{\text{anal}} = \frac{|V_{\mu\nu}^{(0)}|^2}{\hbar^2\Omega}\exp\left[\frac{2\lambda_\alpha\zeta}{\hbar\Omega}\right]\int_{-\infty}^{\infty} d\tau \exp\left[-\frac{1}{2}\chi\tau^2 + p(\cos\tau - 1) + i(q\sin\tau + \theta\tau)\right] \quad (23)$$

where the dimensionless parameters are defined as[29]

$$\zeta = \coth\left(\left(\frac{1}{2}\right)\beta\hbar\Omega\right); \quad \chi = \frac{2\lambda}{\beta\hbar^2\Omega^2}; \quad \theta = \frac{\Delta G^0 + \lambda}{\hbar\Omega}; \quad p = \zeta\frac{\lambda_\alpha}{\hbar\Omega}; \quad q = \frac{\lambda_\alpha}{\hbar\Omega} \quad (24)$$

for symmetric systems with zero reorganization energy along the R coordinate. In eq 24, λ is the solvent reorganization energy and $\lambda_\alpha = \hbar^2\alpha^2/2M$. This formulation of the rate expression is similar to that previously derived for vibrationally nonadiabatic PT reactions occurring on a single adiabatic electronic surface.[42−45] At the end of this subsection, we compare the rates calculated with eqs 5 and 7 to those calculated with eq 23.

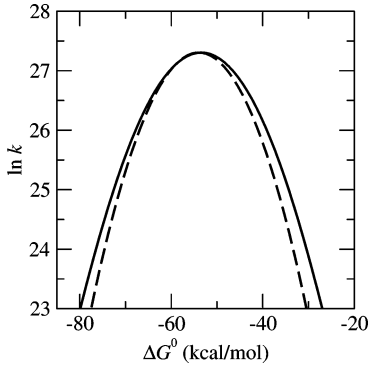

Figure 8. The ln k as a function of the reaction free energy $\Delta G°$ for model 1 with $\alpha = 10$ Å^{-1} (solid) and an inverted parabola calculated with $\ln k \propto -(\Delta G° + \lambda)^2/(4\lambda k_BT)$ using $\lambda = \langle\epsilon\rangle = 53.13$ kcal/mol (dashed). The parabolas were vertically adjusted so that the two maxima correspond to the same rates. The rate constant k is given in s^{-1}.

In addition to the linear response approximation discussed in the previous section, the derivation of the analytical PCET rate expression given in eq 23 depends on two other approximations that can be tested with these molecular dynamics simulations. In the first approximation, the R coordinate motion is assumed to be harmonic, and the solvent damping effects on this harmonic motion are assumed to be negligible. In this case, the R coordinate time correlation function $C_R(t)$ can be replaced with the standard analytical expression for the time correlation function of an undamped quantum mechanical harmonic oscillator. Figure 9a compares the R coordinate term, $F_R(t)$, for $C_R(t)$ calculated with classical molecular dynamics simulations ($F_R^{\text{MD}}(t)$), the classical harmonic oscillator approximation given in eq 14 ($F_R^{\text{cl}}(t)$), and the quantum harmonic oscillator approximation given in eq 13 ($F_R^{\text{q}}(t)$). The similarity between $F_R^{\text{MD}}(t)$ and $F_R^{\text{cl}}(t)$ indicates that anharmonic and solvent damping effects for the R motion are not significant on the time scale of the probability flux. Both $F_R^{\text{cl}}(t)$ and $F_R^{\text{q}}(t)$ are relatively constant on the relevant time scale, implying that the quantum effects of the R coordinate do not impact the dynamical behavior of the probability flux. Inclusion of the quantum effects of the R coordinate, however, slightly increases the magnitude of the rates.

The second approximation used in the derivation of the analytical PCET rate expression is the short-time approximation. In this limit, only the initial value of the energy gap correlation function impacts the rate, so $C_\epsilon(t) \approx C_\epsilon(0) \equiv \langle\delta\epsilon^2\rangle$. This approximation is valid when the decay time of the probability flux $j(t)$ is short with respect to the initial decay time of the energy gap correlation function $C_\epsilon(t)$. According to the short-time approximation, the solvent damping term becomes a Gaussian:

$$\exp\left\{-\frac{1}{\hbar^2}\int_0^t d\tau_1\int_0^{\tau_1} d\tau_2 C_\epsilon(\tau_1 - \tau_2)\right\} = \exp\left\{-\frac{\langle\delta\epsilon^2\rangle t^2}{2\hbar^2}\right\} \quad (25)$$

Figure 9b compares the exact solvent damping term with $C_\epsilon(t)$ calculated from the simulations to the approximate expression in eq 25. These two curves are indistinguishable, indicating that the short-time approximation is valid for these types of systems.

Figure 10 presents a comparison of the probability flux correlation functions calculated from the analytical expression

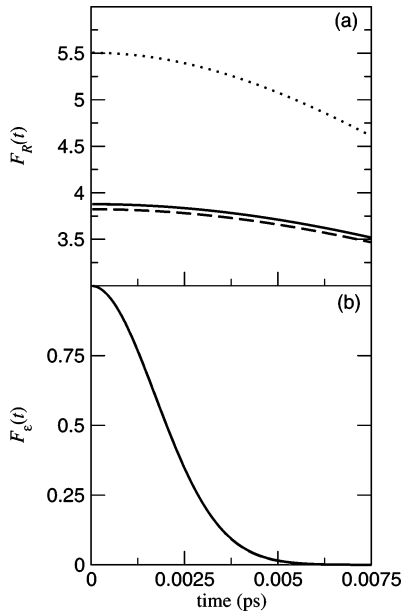

Figure 9. (a) Comparison of the R coordinate term $F_R(t) = \exp\{\alpha_{\mu\nu}^2[C_R(0) + C_R(t)]\}$ for model 1 with $\alpha = 10$ Å^{-1} calculated with $C_R(t)$ from the classical molecular dynamics simulations (solid) to this term with $C_R(t)$ for an undamped quantum harmonic oscillator given in eq 13 (dotted) and with $C_R(t)$ for an undamped classical harmonic oscillator given in eq 14 (dashed). (b) Comparison of the solvent damping term $F_\epsilon(t) = \exp\{-(1/\hbar^2)\int_0^t d\tau_1 \int_0^{\tau_1} d\tau_2\, C_\epsilon(\tau_1 - \tau_2)\}$ for model 1 calculated with classical molecular dynamics simulations (solid) and with the short-time approximation given in eq 25 (dashed). Note that the solid and dashed curves are virtually indistinguishable. The real parts of the complex terms are plotted.

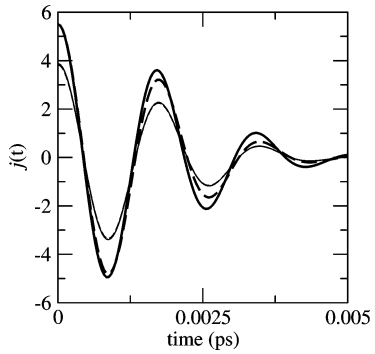

Figure 10. Comparison of the probability flux correlation function $j(t)$, scaled by $|V^{(0)}|^2$, for model 1, with $\alpha = 10$ Å^{-1} using eq 7 with $F_R^{MD}(t)$ (thin solid), $F_R^{cl}(t)$ (thin dashed), and $F_R^{q}(t)$ (thick dashed), and using the analytical expression given in eq 23 (thick solid). The real parts of the complex terms are plotted. Note that the solid and dashed thin lines are virtually indistinguishable.

given by eq 23 and from eq 7 in conjunction with the three different forms of the R coordinate term $F_R^{MD}(t)$, $F_R^{cl}(t)$, and $F_R^{q}(t)$. All of the probability flux correlation functions were calculated for model 1 with $\alpha = 10$Å^{-1}, and $\lambda = \langle\epsilon\rangle$ in the analytical rate expression. The probability flux correlation function calculated from the analytical expression is similar to that calculated from eq 7 using $F_R^{q}(t)$ because $C_R(t)$ is approximated as the time correlation function of an undamped quantum harmonic oscillator in the derivation of the analytical expression. The minor differences between these two curves are due to subtle deviations from linear response theory, as manifested by the quantitative difference between $\langle\epsilon\rangle$ and $\langle\delta\epsilon^2\rangle/2k_BT$. The two curves become virtually indistinguishable if λ is replaced by $\langle\delta\epsilon^2\rangle/2k_BT$ in the $\chi = 2\lambda/\beta\hbar^2\Omega^2$ term of the

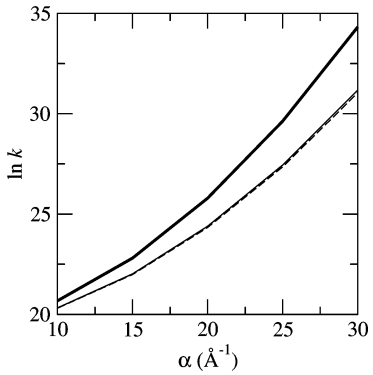

Figure 11. The ln k for model 1 using the probability flux correlation function in eq 7, with $F_R^{MD}(t)$ (thin solid), $F_R^{cl}(t)$ (thin dashed), and $F_R^{q}(t)$ (thick dashed), and using the analytical expression given in eq 23 (thick solid). The rate constant k is given in s^{-1}. Note that the solid and dashed lines are virtually indistinguishable in both cases.

analytical expression. The minor differences between the probability flux correlation functions calculated from eq 7 using $F_R^{MD}(t)$ and $F_R^{cl}(t)$ arise from relatively small anharmonic and solvent damping effects on the R motion (i.e., on $C_R(t)$) in the molecular dynamics simulations.

The α dependence of the rates calculated from the time integration of these probability flux correlation functions is depicted in Figure 11. The rates calculated from the analytical expression are virtually identical to the rates calculated with eq 7 using $F_R^{q}(t)$ for all values of α. Similarly, the rates calculated with eq 7 using $F_R^{MD}(t)$ and $F_R^{cl}(t)$ are nearly indistinguishable.

IV. Conclusions

In this paper, we performed molecular dynamics simulations on a model system to analyze fundamental aspects of PCET reactions in solution. We investigated the impact of the solvent reorganization energy, the proton donor−acceptor frequency, and the distance dependence of the nonadiabatic coupling on the dynamical aspects of the reaction and the magnitude of the rate. We also tested the validity of the linear response approximation for these types of systems and the additional approximations underlying previously derived analytical rate expressions. Furthermore, we compared the rates calculated from the molecular dynamics simulations to those calculated with the analytical rate expression.

Our analysis of the contributions to the nonadiabatic rate constant indicates that the solvent reorganization energy impacts the time dependence of the probability flux correlation function as well as the magnitude of the PCET rate. Increasing the solvent reorganization energy leads to a faster decay of the solvent damping term in the probability flux correlation function. The solvent damping term dominates the decay of the probability flux because it decays to zero much faster than any other component in the probability flux. Thus, the solvent reorganization energy determines the time scale of the probability flux decay. The magnitude of the PCET rate constant, which is calculated by the time integration of the probability flux correlation function, decreases as the solvent reorganization energy increases when all other physical properties remain the same.

In contrast, we found that the proton donor−acceptor frequency strongly impacts the magnitude of the PCET rate but does not significantly influence the time dependence of the probability flux. Decreasing the proton donor−acceptor frequency increases the magnitude of the R coordinate term in the probability flux correlation function and therefore increases the

magnitude of the overall PCET rate. The physical basis for this phenomenon is that a lower proton donor−acceptor frequency enables the sampling of smaller proton donor−acceptor distances, which are associated with significantly larger nonadiabatic couplings. The dynamics of the reaction is not affected by the proton donor−acceptor frequency because the R coordinate term is relatively constant on the time scale of the probability flux decay.

We also found that the distance dependence of the nonadiabatic coupling significantly impacts the magnitude of the PCET rate. The parameter α in the exponential of the nonadiabatic coupling dictates the increase of the nonadiabatic coupling as the proton donor−acceptor distance decreases. Increasing the parameter α increases the magnitude of the R coordinate term in the probability flux correlation function and therefore increases the magnitude of the overall PCET rate. The physical basis for this phenomenon is that a larger value of α leads to larger nonadiabatic couplings for the relevant proton donor−acceptor distances, which are smaller than the equilibrium distance. Moreover, the rate increases faster with α as the proton donor−acceptor frequency decreases because smaller proton donor−acceptor distances are more accessible with a lower proton donor−acceptor frequency.

In addition, we tested the validity of the linear response approximation for these types of PCET systems. The free energy profiles corresponding to the reactant and product vibronic states are nearly parabolic as functions of the energy gap coordinate, and the dependence of the rate on driving force is close to an inverted parabola. The minor deviations from linear response behavior were determined to arise from short-range solvent−solute interactions that are neglected in the linear response approximation. As in electron transfer theory, however, deviations from linear response theory are expected to arise from quantum vibronic effects, different solute polarizabilities for reactant and product states, and solvent nuclear quantum effects.

We also tested additional approximations underlying a previously derived analytical rate expression. The short-time approximation for the solvent was determined to be valid for these types of systems. Moreover, we found that anharmonic and solvent damping effects on the proton donor−acceptor motion are not significant on the time scale of the probability flux. Inclusion of the quantum effects of the proton donor−acceptor motion slightly increases the magnitude of the overall rate but does not impact the dynamical behavior of the probability flux. The rates calculated from the molecular dynamics simulations agree well with those calculated from the analytical rate expression. Thus, these studies provide validation for the use of the previously derived analytical rate expressions.

The analyses presented in this paper enhance our understanding of the fundamental physical principles of PCET reactions in solution. This theoretical formulation for PCET reactions is also applicable to larger, more complex biological systems. Furthermore, the analytical rate expressions enable the prediction of the temperature dependence of the rates and the deuterium kinetic isotope effects for comparison to experiment.

Acknowledgment. We are grateful for support from NSF Grant CHE-0501260 and NIH Grant GM56207.

References and Notes

(1) Babcock, G. T.; Barry, B. A.; Debus, R. J.; Hoganson, C. W.; Atamian, M.; McIntosh, L.; Sithole, I.; Yocum, C. F. *Biochemistry* **1989**, *28*, 9557.

(2) Okamura, M. Y.; Feher, G. *Annu. Rev. Biochem.* **1992**, *31*, 861.

(3) Knapp, M. J.; Rickert, K. W.; Klinman, J. P. *J. Am. Chem. Soc.* **2002**, *124*, 3865.

(4) Sjodin, M.; Styring, S.; Akermark, B.; Sun, L.; Hammarstrom, L. *J. Am. Chem. Soc.* **2000**, *122*, 3932.

(5) Huynh, M. H. V.; Meyer, T. J. *Angew. Chem., Int. Ed.* **2002**, *41*, 1395.

(6) Kirby, J. P.; Roberts, J. A.; Nocera, D. G. *J. Am. Chem. Soc.* **1997**, *119*, 9230.

(7) Farrer, B. T.; Thorp, H. H. *Inorg. Chem.* **1999**, *38*, 2497.

(8) Binstead, R. A.; Meyer, T. J. *J. Am. Chem. Soc.* **1987**, *109*, 3287.

(9) Roth, J. P.; Lovel, S.; Mayer, J. M. *J. Am. Chem. Soc.* **2000**, *122*, 5486.

(10) Siegbahn, P. E. M.; Eriksson, L.; Himo, F.; Pavlov, M. *J. Phys. Chem. B* **1998**, *102*, 10622.

(11) Blomberg, M. R. A.; Siegbahn, P. E. M.; Styring, S.; Babcock, G. T.; Akermark, B.; Korall, P. *J. Am. Chem. Soc.* **1997**, *119*, 8285.

(12) Hoganson, C. W.; Babcock, G. T. *Science* **1997**, *277*, 1953.

(13) Hoganson, C. W.; Lydakis-Simantiris, N.; Tang, X.-S.; Tommos, C.; Warncke, K.; Babcock, G. T.; Diner, B. A.; McCracken, J.; Styring, S. *Photosynth. Res.* **1995**, *47*, 177.

(14) Tommos, C.; Tang, X.-S.; Warncke, K.; Hoganson, C. W.; Styring, S.; McCracken, J.; Diner, B. A.; Babcock, G. T. *J. Am. Chem. Soc.* **1995**, *117*, 10325.

(15) G. T. Babcock, B. A. D.; J. McCracken, S. Styring. *Photosynth. Res.* **1995**, *47*, 177.

(16) Diner, B. A.; Babcock, G. T. Structure, dynamics and energy conversion efficiency in photosystem II. In *Oxygenic Photosynthesis: The Light Reactions*; Ort, D. R., Yocum, C. F., Eds.; Kluwer: Dordrecht, The Netherlands, 1996; p 213.

(17) Babcock, G. T.; Wikstrom, M. *Nature (London)* **1992**, *356*, 301.

(18) Malmstrom, B. G. *Acc. Chem. Res.* **1993**, *26*, 332.

(19) Cukier, R. I. *J. Phys. Chem.* **1994**, *98*, 2377.

(20) Cukier, R. I. *J. Phys. Chem.* **1996**, *100*, 15428.

(21) Cukier, R. I. *J. Phys. Chem. A* **1999**, *103*, 5989.

(22) Cukier, R. I. *J. Phys. Chem. B* **2002**, *106*, 1746.

(23) Cukier, R. I. *Biochim. Biophys. Acta−Bioenerg.* **2004**, *1655*, 37.

(24) Cukier, R. I.; Nocera, D. G. *Annu. Rev. Phys. Chem.* **1998**, *49*, 337.

(25) Hammes-Schiffer, S. *Acc. Chem. Res.* **2001**, *34*, 273.

(26) Soudackov, A.; Hammes-Schiffer, S. *J. Chem. Phys.* **1999**, *111*, 4672.

(27) Soudackov, A.; Hammes-Schiffer, S. *J. Chem. Phys.* **2000**, *113*, 2385.

(28) Hammes-Schiffer, S. Proton-coupled electron transfer. In *Electron Transfer in Chemistry Vol. I. Principles, Theories, Methods, and Techniques*; Balzani, V., Ed.; Wiley-VCH: Weinheim, Germany, 2001; p 189.

(29) Soudackov, A.; Hatcher, E.; Hammes-Schiffer, S. *J. Chem. Phys.* **2005**, *122*, 014505.

(30) Mayer, J. M.; Hrovat, D. A.; Thomas, J. L.; Borden, W. T. *J. Am. Chem. Soc.* **2002**, *124*, 11142.

(31) Mincer, J. S.; Schwartz, S. D. *J. Chem. Phys.* **2004**, *120*, 7755.

(32) Moore, D. B.; Martinez, T. J. *J. Phys. Chem. A* **2000**, *104*, 2367.

(33) Georgievskii, Y.; Stuchebrukhov, A. A. *J. Chem. Phys.* **2000**, *113*, 10438.

(34) Siegbahn, P. E. M.; Blomberg, M. R. A.; Crabtree, R. H. *Theor. Chem. Acc.* **1997**, *97*, 289.

(35) Siebrand, W.; Smedarchina, Z. *J. Phys. Chem. B* **2004**, *108*, 4185.

(36) Kuznetsov, A. M. *Charge Transfer in Physics, Chemistry, and Biology*; Gordon & Breach: Reading, U.K., 1995.

(37) Hatcher, E.; Soudackov, A.; Hammes-Schiffer, S. *Chem. Phys., in press.*

(38) Warshel, A. *Computer Modeling of Chemical Reactions in Enzymes and Solutions*; John Wiley & Sons: New York, 1991.

(39) Hammes-Schiffer, S.; Iordanova, N. *Biochim. Biophys. Acta−Bioenerg.* **2004**, *1655*, 29.

(40) Iordanova, N.; Decornez, H.; Hammes-Schiffer, S. *J. Am. Chem. Soc.* **2001**, *123*, 3723.

(41) Iordanova, N.; Hammes-Schiffer, S. *J. Am. Chem. Soc.* **2002**, *124*, 4848.

(42) Suarez, A.; Silbey, R. *J. Chem. Phys.* **1991**, *94*, 4809.

(43) Trakhtenberg, L. I.; Kochikhim, V. L.; Pshezhetsky, S. Y. *Chem. Phys.* **1982**, *69*, 121.

(44) Borgis, D.; Lee, S.; Hynes, J. T. *Chem. Phys. Lett.* **1989**, *162*, 19.

(45) Borgis, D.; Hynes, J. T. *J. Chem. Phys.* **1991**, *94*, 3619.

(46) Webb, S. P.; Iordanov, T.; Hammes-Schiffer, S. *J. Chem. Phys.* **2002**, *117*, 4106.

(47) Pak, M. V.; Swalina, C.; Webb, S. P.; Hammes-Schiffer, S. *Chem. Phys.* **2004**, *304*, 227.

(48) Chandler, D. *Liquids Freezing and Glass Transition*; Elsevier: Amsterdam, 1991; Vol. 51.

(49) Jorgensen, W. L. *J. Am. Chem. Soc.* **1981**, *103*, 335.

(50) Jorgensen, W. L.; Chandreskhar, J.; Madura, J. D.; Impey, R. W.; Klein, M. L. *J. Chem. Phys.* **1982**, *79*, 926.

(51) Cornell, W. D.; Cieplak, P.; Bayly, C. I.; Gould, I. R.; Merz, K. M.; Ferguson, D. M.; Spellmeyer, D. C.; Fox, T.; Caldwell, J. W.; Kollman, P. A. *J. Am. Chem. Soc.* **1995**, *117*, 5179.
(52) Ewald, P. P. *Ann. Phys.* **1921**, *64*, 253.
(53) Smith, W.; Forester, T. R. DL_POLY_2.14; CCLRC, Daresbury Laboratory: Warrington, England, 2003.
(54) Verlet, L. *Phys. Rev.* **1967**, *159*, 98.
(55) Ryckaert, J. P.; Ciccotti, G.; Berendsen, H. J. C. *J. Comput. Phys.* **1977**, *23*, 327.
(56) Hoover, W. G. *Phys. Rev. A* **1985**, *31*, 1695.
(57) Ando, K. *J. Chem. Phys.* **1997**, *106*, 116.
(58) Marcus, R. A. *Annu. Rev. Phys. Chem.* **1964**, *15*, 155.
(59) Warshel, A. *J. Phys. Chem.* **1982**, *86*, 2218.
(60) Hwang, J.-K.; Warshel, A. *J. Am. Chem. Soc.* **1987**, *109*, 715.
(61) M. Bixon, J. J. *J. Phys. Chem.* **1991**, *95*, 1941.
(62) S. Efrima, M. B. *Chem. Phys.* **1976**, *13*, 447.
(63) Matyushov, D. V.; Voth, G. A. *J. Chem. Phys.* **2000**, *113*, 5413.
(64) Small, D. W.; Matyushov, D. V.; Voth, G. A. *J. Am. Chem. Soc.* **2003**, *125*, 7470.
(65) Ando, K. *J. Chem. Phys.* **2001**, *114*, 9470.